Study of Excited Ξ Baryons in $\bar{p}p$-Collisions with $\overline{\mathrm{P}}$ANDA

Authors:

Jennifer Pütz, Albrecht Gillitzer, James Ritman

Abstract

Understanding the excitation pattern of baryons is indispensable for a deep insight into the mechanism of non-perturbative QCD. Up to now only the nucleon excitation spectrum has been subject to systematic experimental studies while very little is known on excited states of double or triple strange baryons.
In studies of antiproton-proton collisions the $\overline{\mathrm{P}}$ANDA experiment is well-suited for a comprehensive baryon spectroscopy program in the multi-strange and charm sector. A large fraction of the inelastic $\bar{\mathrm{p}}\mathrm{p}$ cross section is associated to final states with a baryon-antibaryon pair together with additional mesons, giving access to excited states both in the baryon and the antibaryon sector.
In the present study we focus on excited Ξ states. For final states containing a $\Xi\,\bar{\Xi}$ pair cross sections up to the order of μb are expected, corresponding to production rates of $\sim 10^6$/d at a Luminosity $L = 10^{31}\,\mathrm{cm}^{-2}\,\mathrm{s}^{-1}$ (5% of the full value). A strategy to study the excitation spectrum of Ξ baryons in antiproton-proton collisions will be discussed. The reconstruction of reactions of the type $\bar{\mathrm{p}}\mathrm{p} \to \Xi^{*}\,\bar{\Xi}$ (and their charge conjugated) with the $\overline{\mathrm{P}}$ANDA detector will be presented based on a specific exemplary reaction and decay channel.

Contents

1 Event generation

To study excited Ξ baryons the simulation of signal events is needed. For this study 1.5 million signal events have been generated. The decay channel for the simulation is shown in figure 1.1.

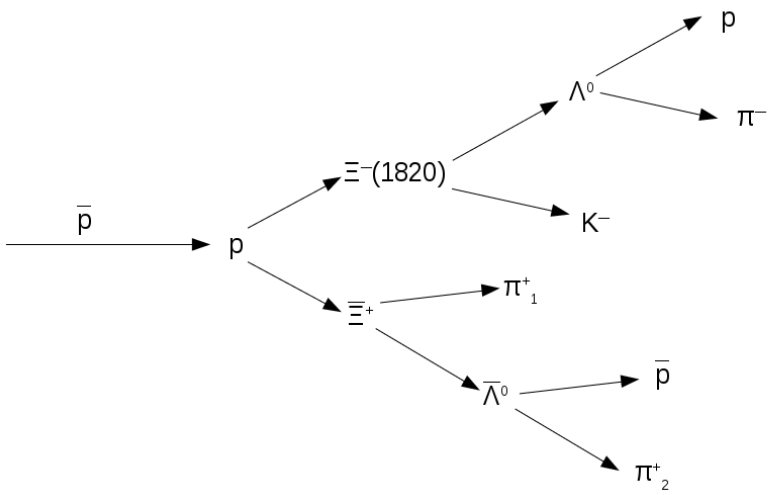

Figure 1.1: Simulated decay channel

For the charge conjugated channel another 1.5 million events were generated. Table 1.1 shows the parameters which are used for the event generation.
The PHPS model is used for the production, because other models are not tested yet. But this is not effecting the strategy for this study.
The chosen beam momentum of $p_{\bar{p}} = 4.6\,\mathrm{GeV/c}$ is 100 MeV above the production threshold of $\Xi\,(1820)$ and $\bar{\Xi}$. The production cross section is expected to be of the same order ($\sim \mu$b) as for Ξ [1].

Table 1.1: Parameter for event generation

Parameter	Value
Beam momentum	4.6 GeV/c^2
Production	PHSP
Tracking	Ideal
Particle ID	Ideal

Table 1.2: Used software versions

Software	Version
FairSoft	mar15
FairRoot	v-15.03a
PandaRoot	trunk revision 28555
Geant	3
Genfit	1

The used software versions for PandaRoot and the external software package is listed in table 1.2

Since now $\Xi(1820)$ was not defined in the evt.pdl file. How the particle is added to the file is shown in the code snippet 1.1. The properties of $\Xi(1820)$ are listed in table 1.3.

Listing 1.1: snippet from evt.pdl

```
add  p Particle Xi(1820)- 23314 1.8230000e+00 2.4000000e-02
    2.0000000e-01 -3 3 0.0000000e+00 23314
add  p Particle anti-Xi(1820)+ -23314 1.8230000e+00 2.4000000e-02
     2.0000000e-01 3 3 0.0000000e+00 -23314
```

Table 1.3: Properties of $\Xi(1820)$ and $\bar{\Xi}(1820)$. The values are taken from [2]

Particle	J	I	P	Charge	Mass	Width
$\Xi(1820)$	$\frac{3}{2}$	$\frac{1}{2}$	(-1)	(-1)	(1.823 ± 5)GeV/c^2	(0.024 ± 6) GeV
$\bar{\Xi}(1820)$	$\frac{3}{2}$	$\frac{1}{2}$	(-1)	1	(1.823 ± 5)GeV/c^2	(0.024 ± 6) GeV

The generated transverse momentum against the longitudinal momentum for Λ^0, $\bar{\Lambda}^0$, $\bar{\Xi}$ and $\Xi(1820)$ is presented in figure 1.2

Figure 1.4 shows the Dalitz plot for the Λ^0, K^- and $\bar{\Xi}$ final states for the channel $\bar{p}p \rightarrow \Xi(1820)\,\bar{\Xi}$.

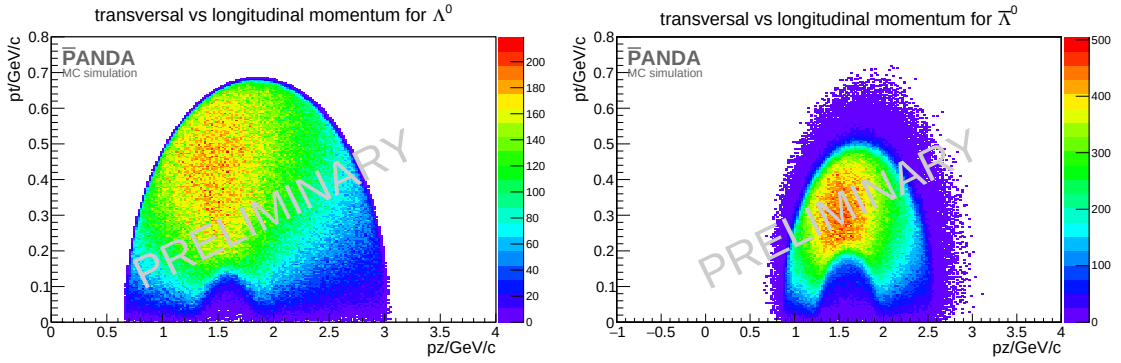

(a) Λ^0 (b) $\bar{\Lambda}^0$

Figure 1.2: "PROPOSED FOR RELEASE" Figure a) shows the transverse momentum on the y axis against the longitudinal momentum on the x axis for Λ^0. Figure b) shows the same distribution for $\bar{\Lambda}^0$.

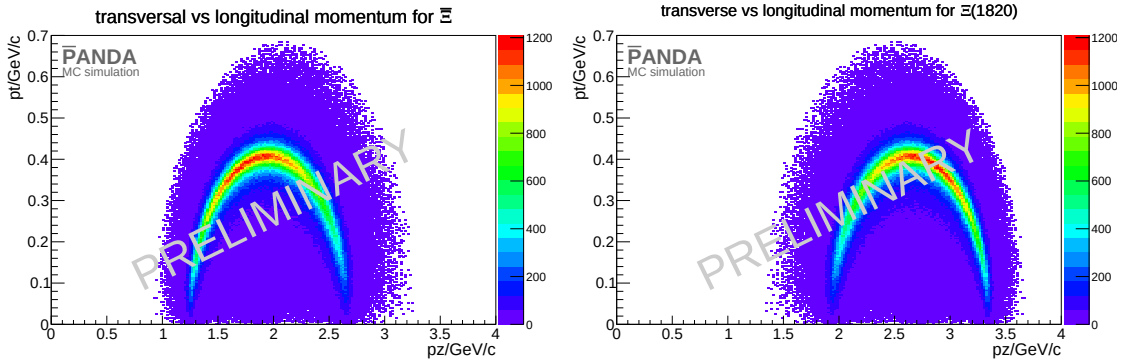

(a) $\bar{\Xi}$ (b) $\Xi\,(1820)$

Figure 1.3: "PROPOSED FOR RELEASE" Figure a) shows transverse against the longitudinal momentum distribution for $\bar{\Xi}$. Figure b) transverse versus longitudinal momentum distribution for $\Xi\,(1820)$.

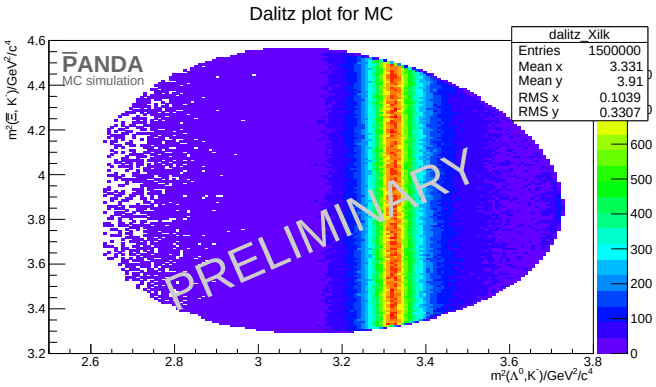

Figure 1.4: "PROPOSED FOR RELEASE" Dalitz plot for simulation. On x axis is the mass square of Λ^0 and K^- and on the y axis there is the mass square of $\bar{\Xi}$ and K^-

2 Analysis

To reconstruct all the simulated particles we start with the final state particles and go backwards through the reaction chain.

2.1 Final state particle

The selected final state particle are protons, anti-proton, π^-, π^+, K^- and K^+ mesons. For the reconstruction of these particles an ideal tracking was used. To make the selection a bit more realistic only particles with more than 3 hits in any inner tracking detector (MVD, STT and GEM) are selected. The selection criterion is chosen because three hits are defining a circle. A fourth hit point is than a validation of the track hypothesis.
The particle identification (PID) is also ideal. The selection criterion is set to 'best'.

The reconstruction efficiency for the final state particle is shown in table 2.1 and figure 2.1.
Table 2.2 shows the reconstruction efficiency for the c.c. channel.

2.2 Reconstruction of Λ^0 and $\bar{\Lambda}^0$

Selection

For the reconstruction of Λ^0 a proton and a π^- meson are combined and for the reconstruction of $\bar{\Lambda}^0$ a $\bar{p}$ and a π^+ are combined. After combining the daughter particles a mass

Table 2.1: "PROPOSED FOR RELEASE" Reconstruction efficiency and momentum resolution for $\bar{p}p \to \Xi(1820)\,\bar{\Xi}$

final state	N/%	$\frac{\sigma p}{p}$/%
π^-	83.48	1.53
π_1^+ ($\bar{\Xi}$)	80.93	1.38
π_2^+ ($\bar{\Lambda}^0$)	83.07	1.49
K^-	78.59	1.58
p	84.39	1.61
$\bar{p}$	78.25	1.61

Table 2.2: "PROPOSED FOR RELEASE" Reconstruction efficiency and momentum resolution for $\bar{p}p \rightarrow \bar{\Xi}(1820)\,\Xi$

final state	N/%	$\frac{\sigma p}{p}$/%
π^+	82.9625	1.54131
π_1^- (Ξ)	80.395	1.37697
π_2^- (Λ^0)	82.6867	1.48918
K^+	83.2709	1.57882
p	80.7079	1.55197
$\bar{p}$	80.9253	1.60091

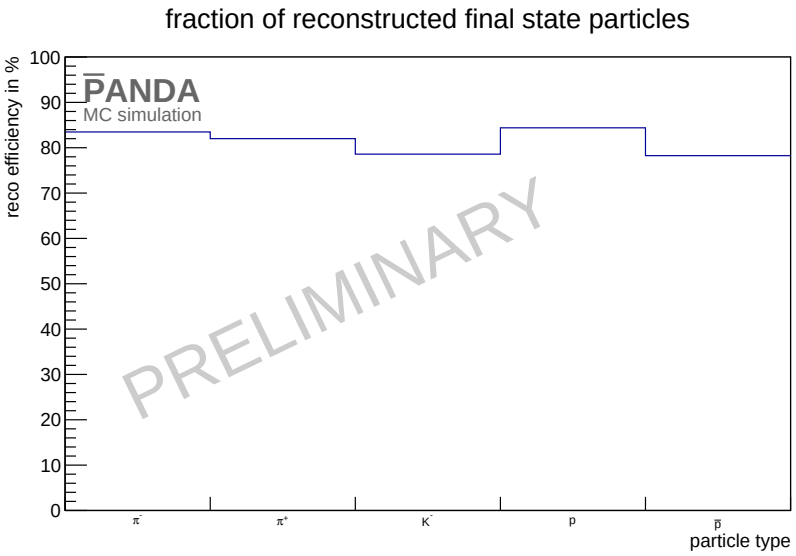

Figure 2.1: "PROPOSED FOR RELEASE" Reconstruction efficiency for final state particles. The x axis shows the particle type. On the y axis is shown the fraction of reconstructed particles, like it is shown in table 2.1

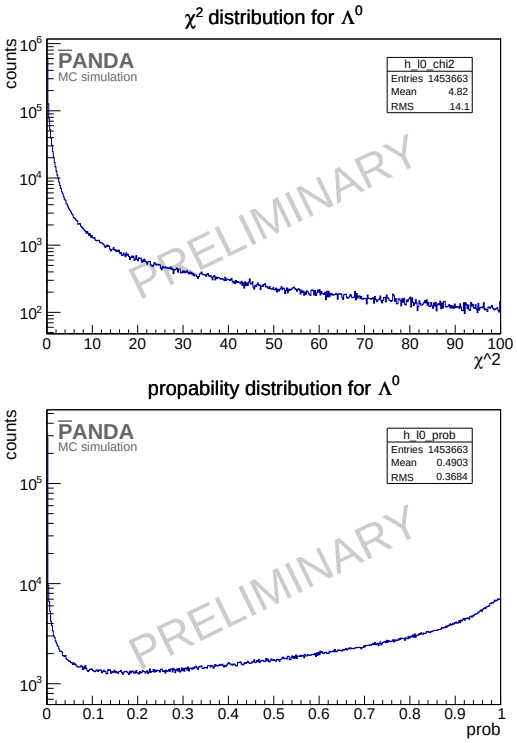

Figure 2.2: "PROPOSED FOR RELEASE" upper: χ^2 distribution; lower: χ^2 probability distribution

window cut is performed. Only those particles are chosen which have a mass within a window of 0.3GeV/c^2 which means $1.116 \pm 0.15\text{GeV/c}^2$.

A vertex constraint fit with the PndKinVtxFitter is performed on the selected particle. This means that the tracks of the daughter particles are fitted to a common vertex point. The χ^2 and χ^2-Probability distribution of the vertex fit for Λ^0 is shown in figure 2.2.

In the χ^2-probability distribution one can see a increasing number of events for probabilities going to one. These feature is not coming from vertex fitting. There is still a problem with covariance matrices which causes the effect.

The fit information coming from the vertex fit are used to perform a mass constraint fit with the kinematic fitter PndKinFitter. After using both fitter the selection criterion is set. One select only those particles which have a probability greater than 1% in both fitter. A scheme which shows how the events are selected can be found in figure 2.3.

If there is more than one candidate left after these cuts, the best fitted candidate is chosen.

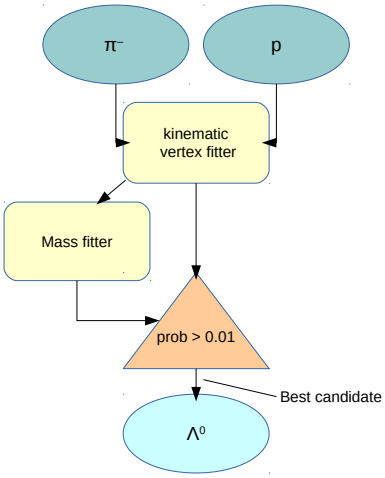

Figure 2.3: propose Scheme for Λ^0 reconstruction

Results

In this paragraph the results for the Λ^0 and $\bar{\Lambda}^0$ selection are presented. The mass distributions for different cuts are shown in figure 2.4 and figure 2.5.
The reconstructed mass can be determined by performing a double Gaussian fit on mass after all cuts. The mass distribution and the double Gaussian fit are exemplarily shown for Λ^0 in figure 2.6
The mean value of the inner Gaussian fit is the reconstructed mass. The result for Λ^0 is $m_{\Lambda^0} = \left(1.116 \pm 3.5 \cdot 10^{-5}\right)$ GeV/c^2 and for $\bar{\Lambda}^0$: $m_{\bar{\Lambda}^0} = \left(1.116 \pm 1 \cdot 10^{-5}\right)$GeV/c^2. The small fit errors could be a result from the wrong covariance matrices. But this has to be checked. Figure 2.7 shows the transverse momentum versus the longitudinal momentum.
After all cuts the reconstruction efficiency for Λ^0 is 50.33% and for $\bar{\Lambda}^0$ 41.46%. The difference of the reconstruction efficiency of Λ^0 and $\bar{\Lambda}^0$ is caused by the difference between the decay length of their mother particles. Λ^0 is emitted by the $\Xi\,(1820)$ which has a very short decay length while the decay length of Ξ and $\bar{\Xi}$ is $c\tau = 4.91\,\text{cm}$ [2]. The decay length of Λ^0 and $\bar{\Lambda}^0$ is $c\tau = 7.98\,\text{cm}$, so that the final state particles of $\bar{\Lambda}^0$ are produced more downstream than the final state particles of Λ^0. This can be also seen in figure 2.8. The finale state particles coming from $\bar{\Lambda}^0$ are produced at the edge of the MVD detector so that the reconstruction efficiency for this particles get worse.

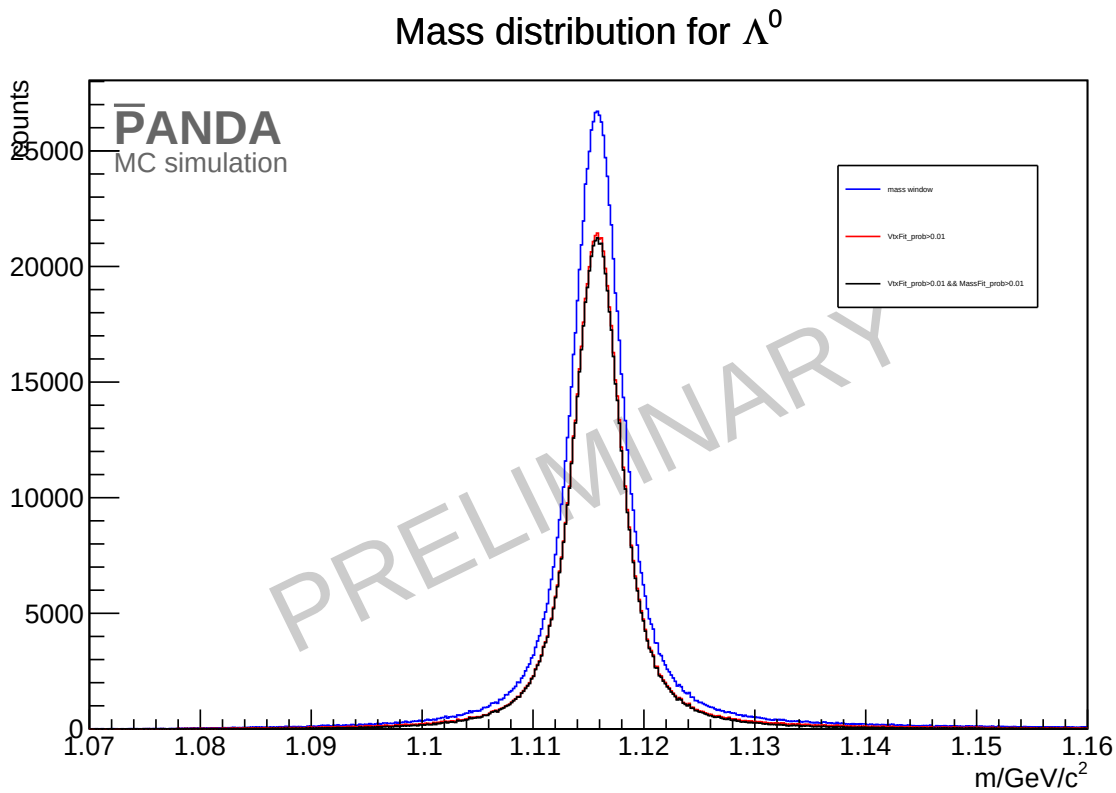

Figure 2.4: "PROPOSED FOR RELEASE" Mass distribution of Λ^0 after the mass window cut in blue, after the vertex fit cut in red and after all cuts in black.

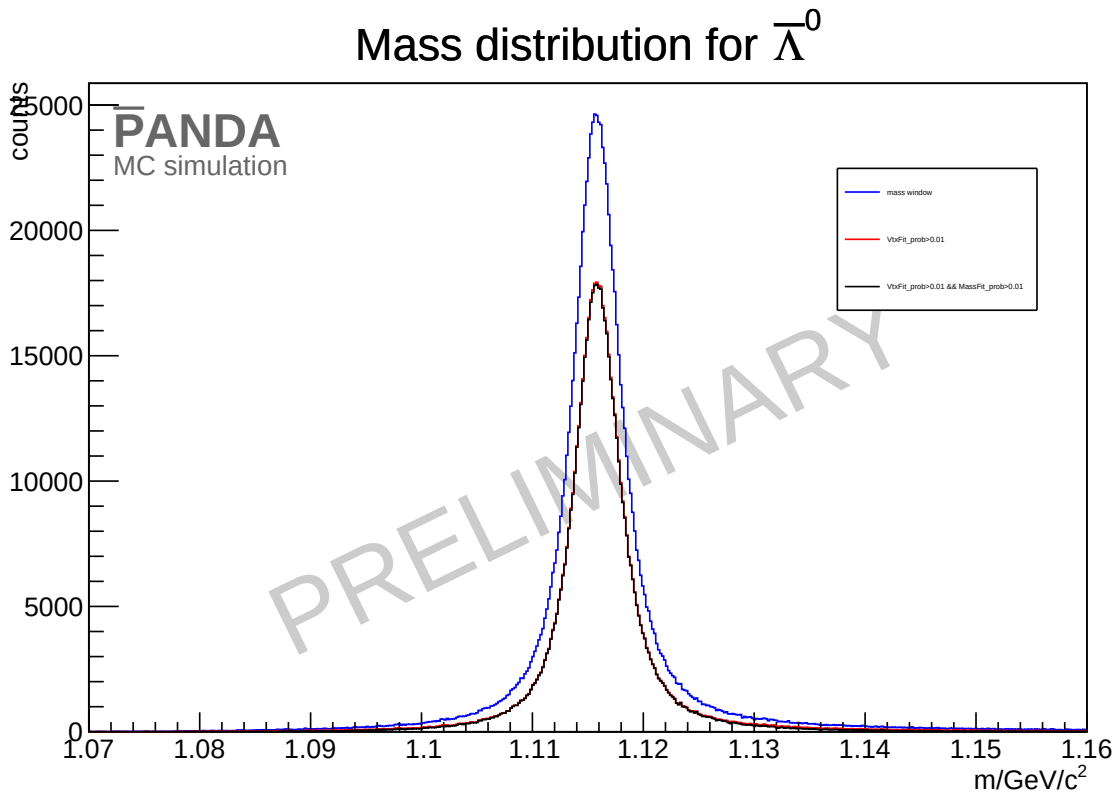

Figure 2.5: "PROPOSED FOR RELEASE" Mass distribution of $\bar{\Lambda}^0$ for different cuts. The blue line shows the the distribution after the mass window cut, the red line after the vertex cut and the black line describes the distribution after all cuts.

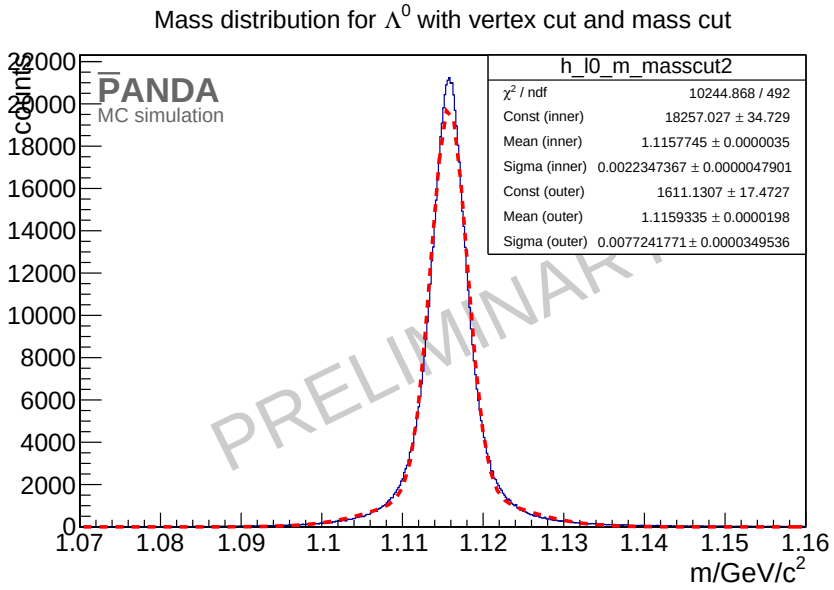

Figure 2.6: "PROPOSED FOR RELEASE" Mass distribution – blue line – for Λ^0 fitted with a double Gaussian fit shown as red dashed line.

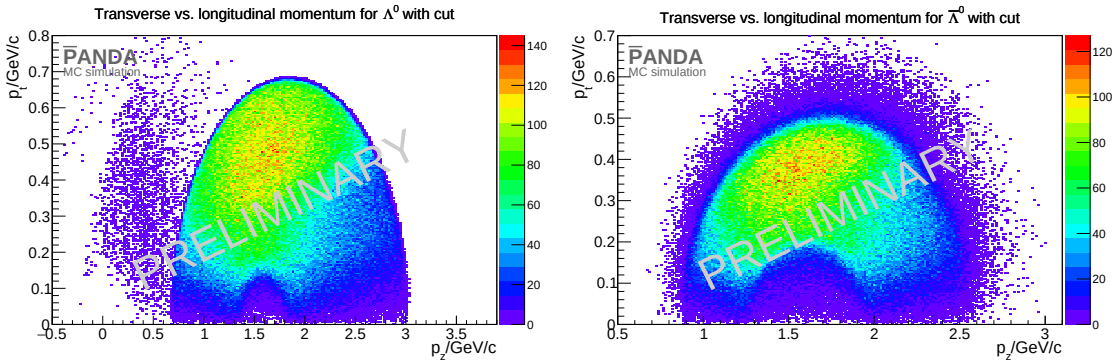

(a) (b)

Figure 2.7: "PROPOSED FOR RELEASE" Figure a) shows the transverse against the longitudinal momentum for Λ^0. Figure b) hows the same distribution for $\bar{\Lambda}^0$.

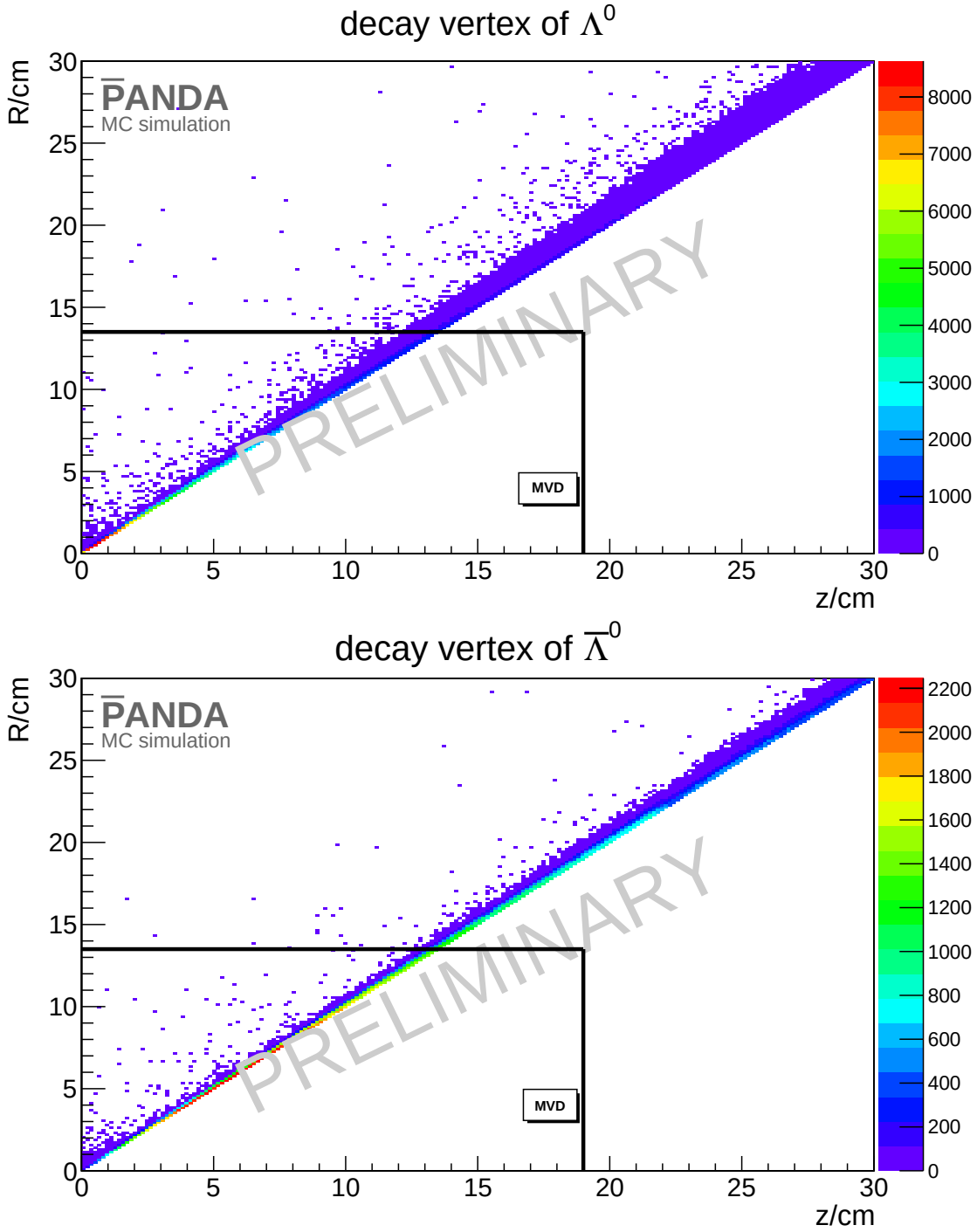

Figure 2.8: "PROPOSED FOR RELEASE" The upper plot shows the decay vertex position of Λ^0 and the lower plot shows the decay vertex position of $\bar{\Lambda}^0$. The x axis of both plots shows the distance of the decay vertex from the interaction point. The y axes show the radius of the decay vertex. The black horizontal and vertical lines mark the borders of the MVD.

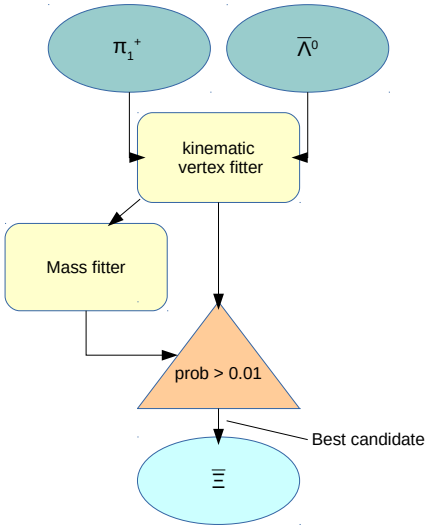

Figure 2.9: "PROPOSED FOR RELEASE" Scheme for $\bar{\Xi}$ reconstruction

2.3 Reconstruction of Ξ and $\bar{\Xi}$

Selection

The reconstruction of Ξ and $\bar{\Xi}$ follows a similar scheme like the reconstruction of Λ^0 and $\bar{\Lambda}^0$. For $\bar{\Xi}$ are $\bar{\Lambda}^0$ and π_1^+ recombined and for Ξ in the c.c. channel Λ^0 and π_1^-. Now it is distinguished between the to π^+ (π^-) particle and use only those particles which have not already been combined. After combining the daughter particles a mass window cut is performed with width of 0.3GeV/c^2 around the Ξ mass $m_\Xi = 1.32171$ GeV/c^2 [2].

The fitting scheme is the same as for Λ^0 and $\bar{\Lambda}^0$ and is shown in figure 2.9 After the mass window cut the daughter particles are fitted to a common vertex with the PndKinVtxFitter. And again these information is used to perform the mass constraint fit.

Only those particles are selected which have a χ^2 probability of more than 1 % in both fitter. Figure 2.10 shows exemplarily the cut on the vertex fit probability.

If there is more than one candidate left after all cuts, the best candidate is chosen.

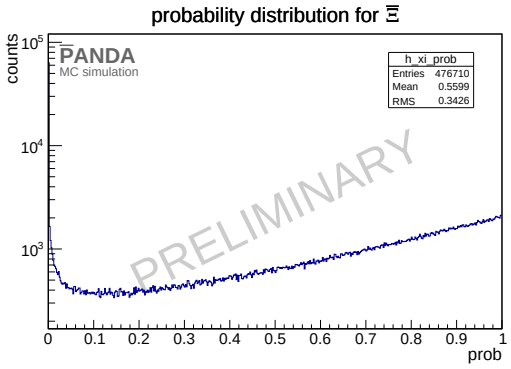

Figure 2.10: "PROPOSED FOR RELEASE" χ^2 probability for $\bar{\Xi}$ reconstruction

Table 2.3: "PROPOSED FOR RELEASE" Vertex resolution for $\bar{\Xi}$ and Ξ (c.c. channel)

position	$\bar{\Xi}$	Ξ (from c.c.)
x/cm	0.052	0.056
y/cm	0.052	0.052
z/cm	0.192	0.2

Results

The vertex resolution after all cuts is shown in table 2.3.

It is determined by calculating the full width at half maximum (FWHM) of the distribution. The advantage of using this method for calculating the vertex resolution is that the FWHM is independent of distribution shape. Figure 2.11 and Figure 2.12 show the vertex resolution.

The mass distribution for the different cuts is shown in figure 2.13 and figure 2.14. The number of events is strongly reduced by the cut on the vertex fit probability. The width of the mass distribution gets smaller.

After using all cuts on the mass distribution the reconstructed mass of Ξ and $\bar{\Xi}$ can be determined by a double Gaussian fit. This is exemplarily shown for the Ξ in figure 2.15.

The result of the mass fit is for $\bar{\Xi}$ m $= \left(1.321716 \pm 9.2 \cdot 10^{-6}\right)$ GeV/c^2 and for Ξ m $= \left(1.3216474 \pm 9.3 \cdot 10^{-6}\right)$GeV/c^2. The two dimensional momentum distribution for $\bar{\Xi}$ and Ξ is shown in figure 2.16

The reconstruction efficiency for $\bar{\Xi}$ is 18.39% and for Ξ 18.64%.

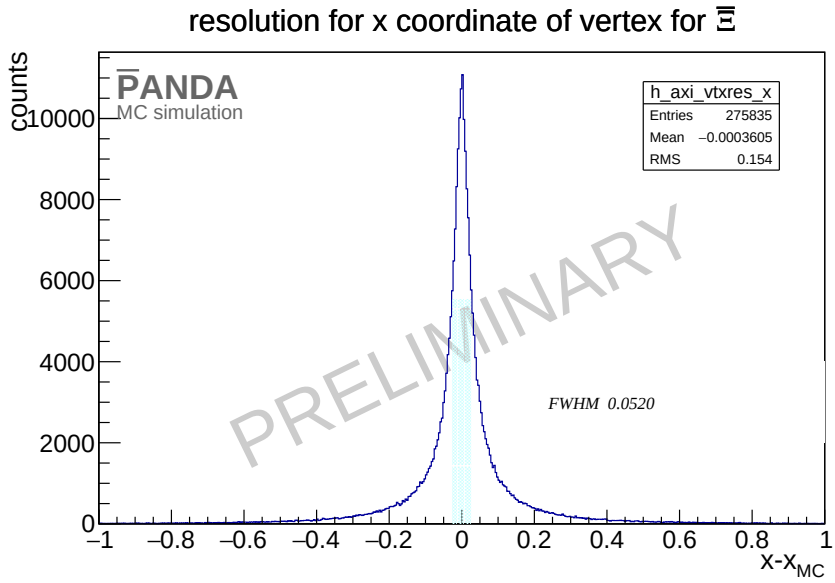

Figure 2.11: "PROPOSED FOR RELEASE" Vertex resolution of x position for $\bar{\Xi}$

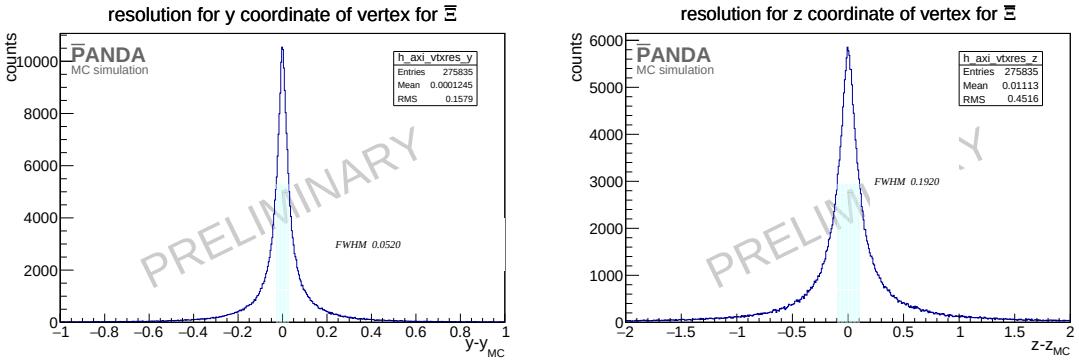

(a) Vertex resolution for y coordinate

(b) Vertex resolution for z coordinate

Figure 2.12: "PROPOSED FOR RELEASE" The left plot shows the vertex resolution of y position for $\bar{\Xi}$. The right plot shows the vertex resolution of z position for $\bar{\Xi}$.

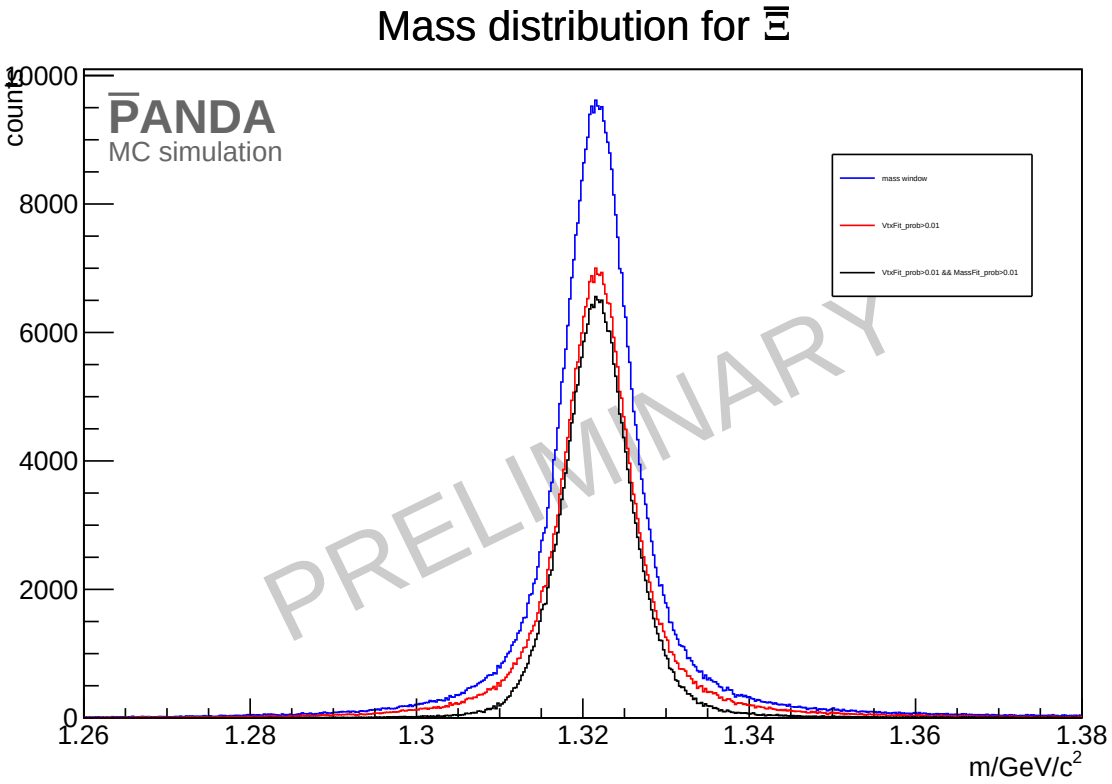

Figure 2.13: "PROPOSED FOR RELEASE" Mass distribution of $\bar{\Xi}$ for different cuts: the mass window cut is shown in blue, the vertex fit cut is shown in red and the distribution after all cuts is shown in black.

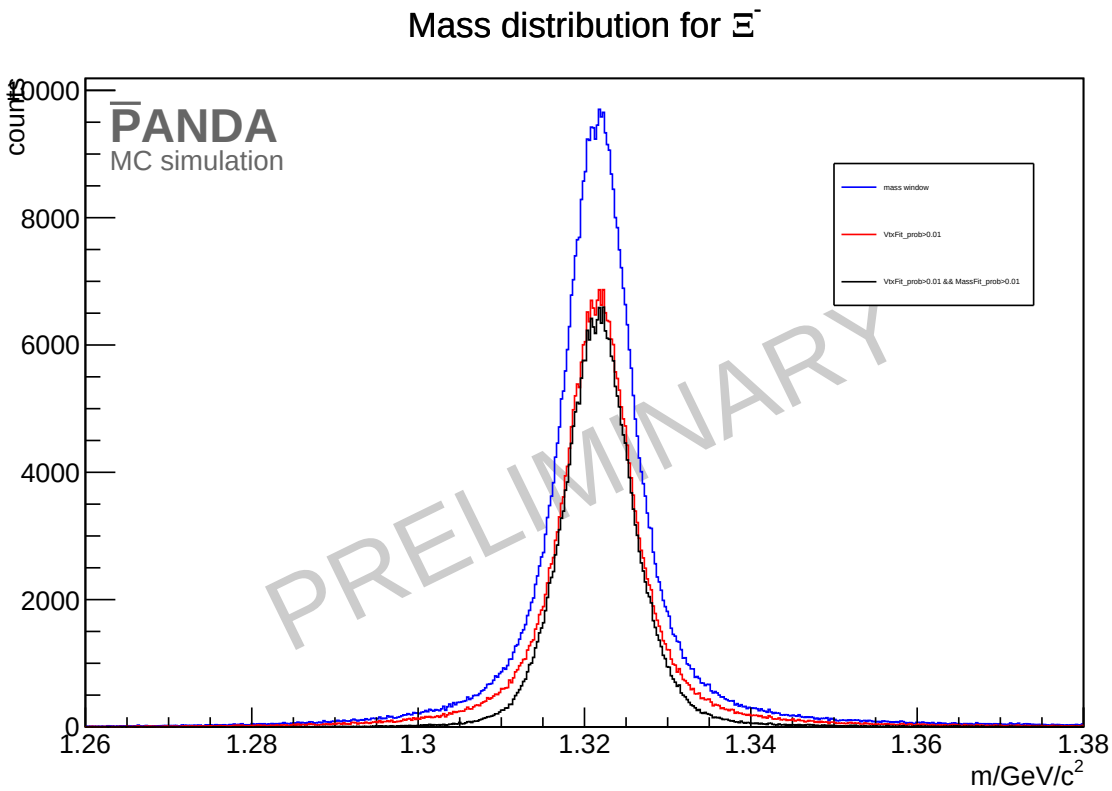

Figure 2.14: "PROPOSED FOR RELEASE" Mass distribution of Ξ for different cuts: mass window cut in blue, vertex fit cut in red and all cuts in black.

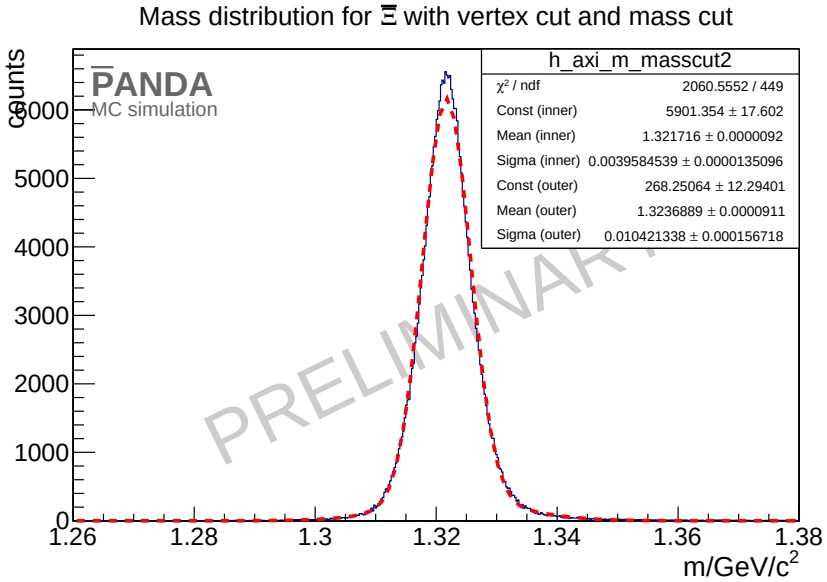

Figure 2.15: "PROPOSED FOR RELEASE" The plot shows the mass distribution (blue line) after all cuts. A double Gaussian fit (red dashed line) is performed to determine the reconstructed mass for the $\bar{\Xi}$.

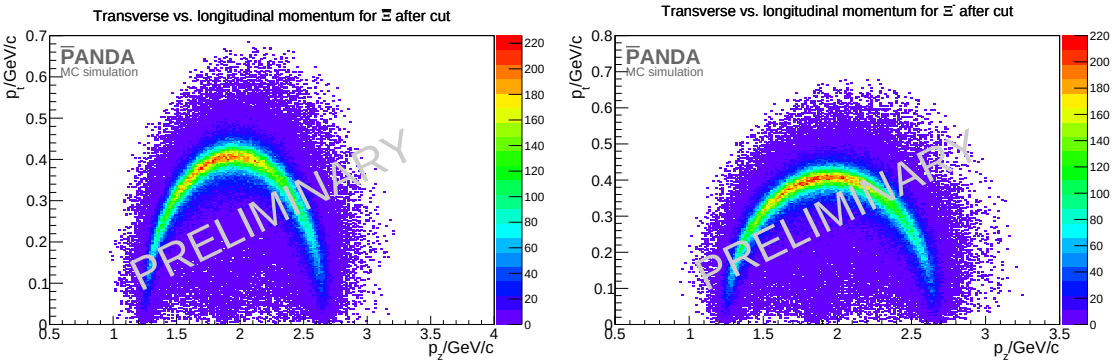

(a) $\bar{\Xi}$ (b) Ξ

Figure 2.16: "PROPOSED FOR RELEASE" The plots shows the transverse against the longitudinal momentum for $\bar{\Xi}$ and Ξ

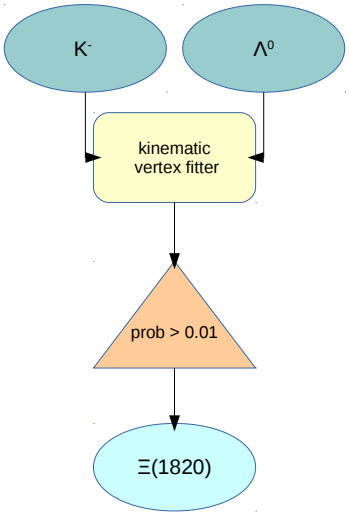

Figure 2.17: "PROPOSED FOR RELEASE" Scheme for Ξ (1820) reconstruction

2.4 Reconstruction of Ξ(1820) and Ξ̄(1820)

Selection

For the reconstruction of Ξ (1820) one combine Λ^0 and K^- meson and for $\bar{\Xi}$ (1820) $\bar{\Lambda}^0$ and K^+ using the best candidate from Λ^0 and $\bar{\Lambda}^0$. After the combination of the particles a mass window cut with width of $0.3 GeV/c^2$ is performed. The daughter particles are fitted then to a common vertex point with the PndKinVtxFitter. Only those candidates for Ξ (1820) ($\bar{\Xi}$ (1820)) are selected which have a fit probability of more then 1%. The selection scheme is shown in figure 2.17.
The χ^2 probability distribution for the vertex fit is shown in figure 2.18. The distribution is again not flat but increases for values up to one.
If there is more than one particle the best candidate is chosen.

Results

The vertex resolution for Ξ (1820) and $\bar{\Xi}$ (1820) is summarized in table 2.4.
Here again the vertex resolution is calculated with the FWHM. This is exemplarily shown

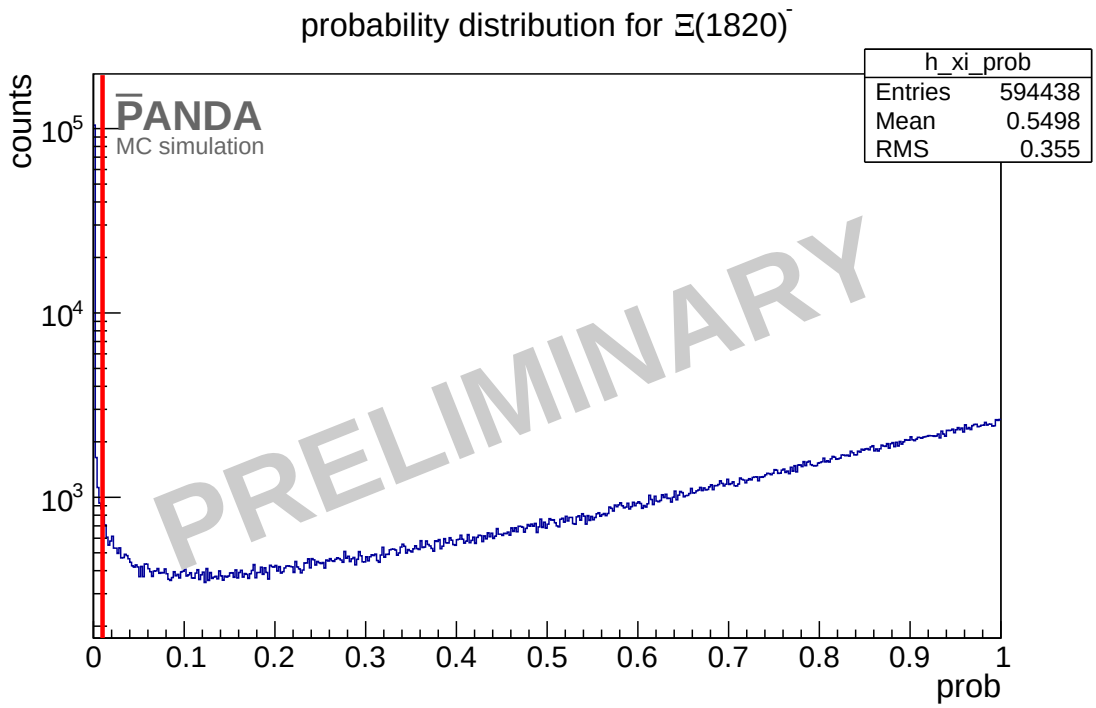

Figure 2.18: "PROPOSED FOR RELEASE" χ^2 probability distribution of kinematic vertex fit for $\Xi\,(1820)$.

Table 2.4: "PROPOSED FOR RELEASE" Vertex resolution for $\Xi\,(1820)$ and $\bar{\Xi}\,(1820)$.

position	$\Xi\,(1820)$	$\bar{\Xi}\,(1820)$ (from c.c.)
x/cm	0.028	0.028
y/cm	0.028	0.028
z/cm	0.1	0.1

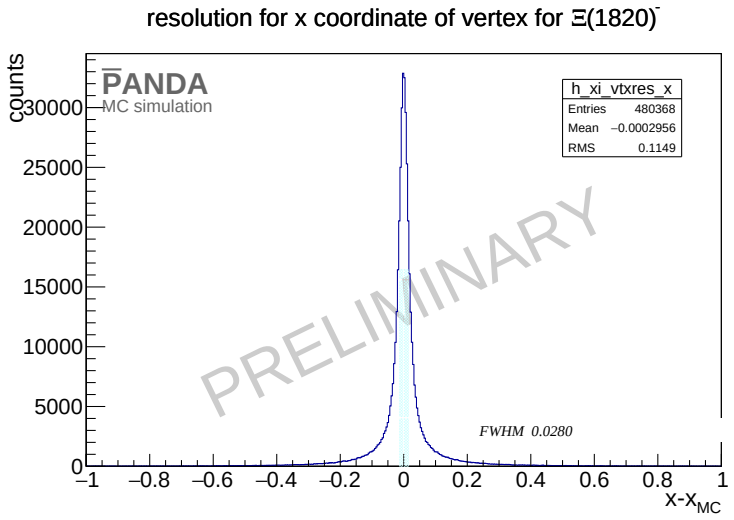

Figure 2.19: "PROPOSED FOR RELEASE" Vertex resolution of the x coordinate for $\Xi\,(1820)$.

for $\Xi\,(1820)$ in figure 2.19 and figure 2.20.

After performing both fits and cut on the probability values, the mass for $\Xi\,(1820)$ and $\bar{\Xi}\,(1820)$ can be determined by fitting with a double Gaussian function. Figure 2.21 shows the mass distribution for both particles after each cut.

The mass fit is exemplarily shown for the $\Xi\,(1820)$ in figure 2.22.

The mass value for the $\Xi\,(1820)$ is fitted to $m_{\Xi^*} = 1.8229 \pm 3.81 \cdot 10^{-5}$ GeV/c^2 and for $\bar{\Xi}\,(1820)$ to $m_{\bar{\Xi}^*} = 1.823 \pm 3.73 \cdot 10^{-5}$ GeV/c^2. These values are close to the input value. Figure 2.23 shows the two dimensional momentum distribution. For both subplots the x axis shows the longitudinal momentum and on the y axis there is shown the transverse momentum.

The reconstructed distributions are in good agreement with the distribution coming from the simulated events which are shown in figure 1.3 (b).

2.5 Reconstruction of the hole reaction chain

Selection

To reconstruct the hole reaction chain $\Xi\,(1820)$ and $\bar{\Xi}$ are combined. This is also done with $\bar{\Xi}\,(1820)$ and Ξ for the charge conjugated channel. For this reconstruction the event selection is done with a exclusive method. The resulting four-momentum vector of both daughter particles – here $\Xi\,(1820)$ and $\bar{\Xi}$ and there c.c. particles – is fitted to the initial for momentum vector

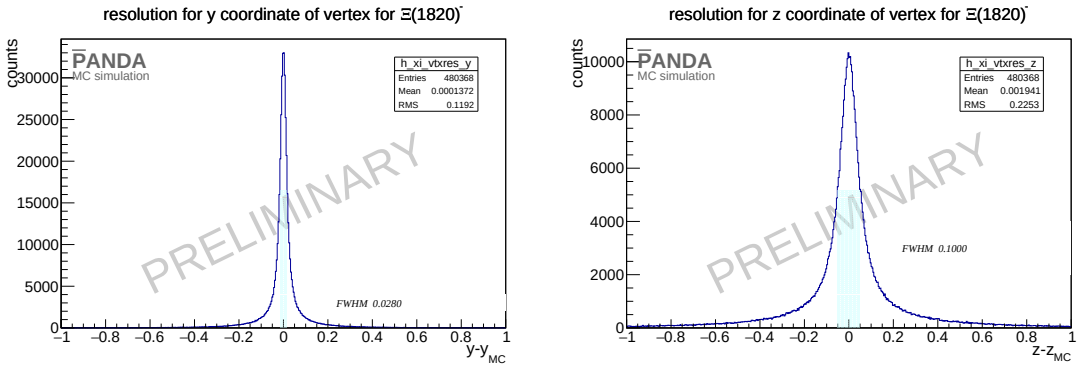

(a) Vertex resolution of the y coordinate for Ξ (1820). (b) Vertex resolution of the z coordinate for Ξ (1820).

Figure 2.20: "PROPOSED FOR RELEASE" Figure a) shows the vertex resolution for the y coordinate and figure b) for the z coordinate of Ξ (1820)

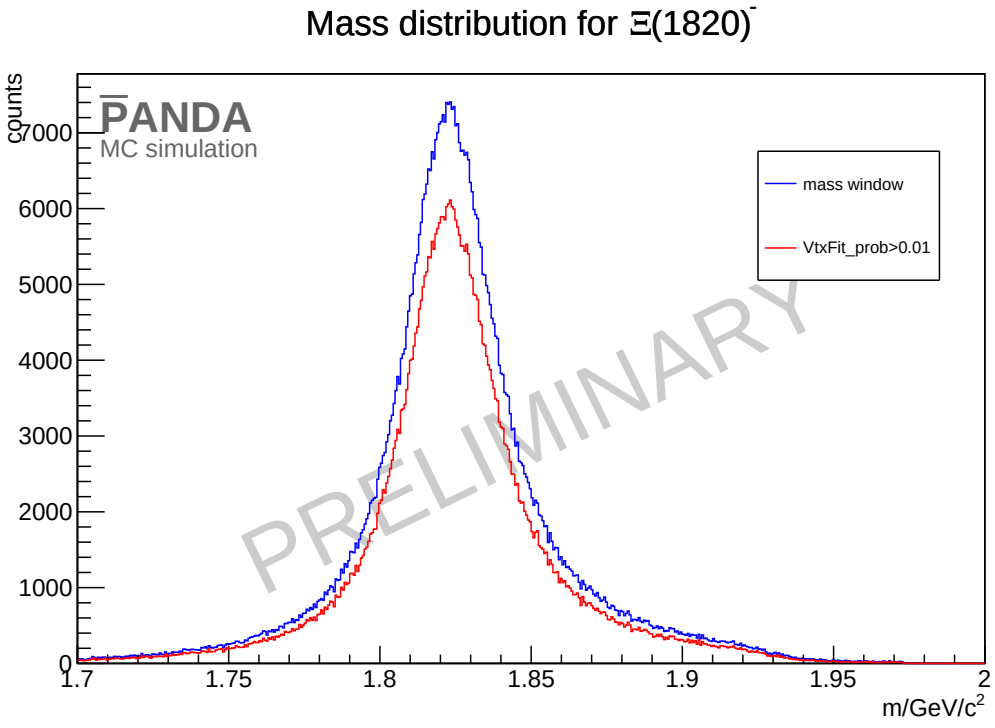

Figure 2.21: "PROPOSED FOR RELEASE" Mass distribution for Ξ (1820) after the mass window cut in blue and after the vertex fit probability cut in red.

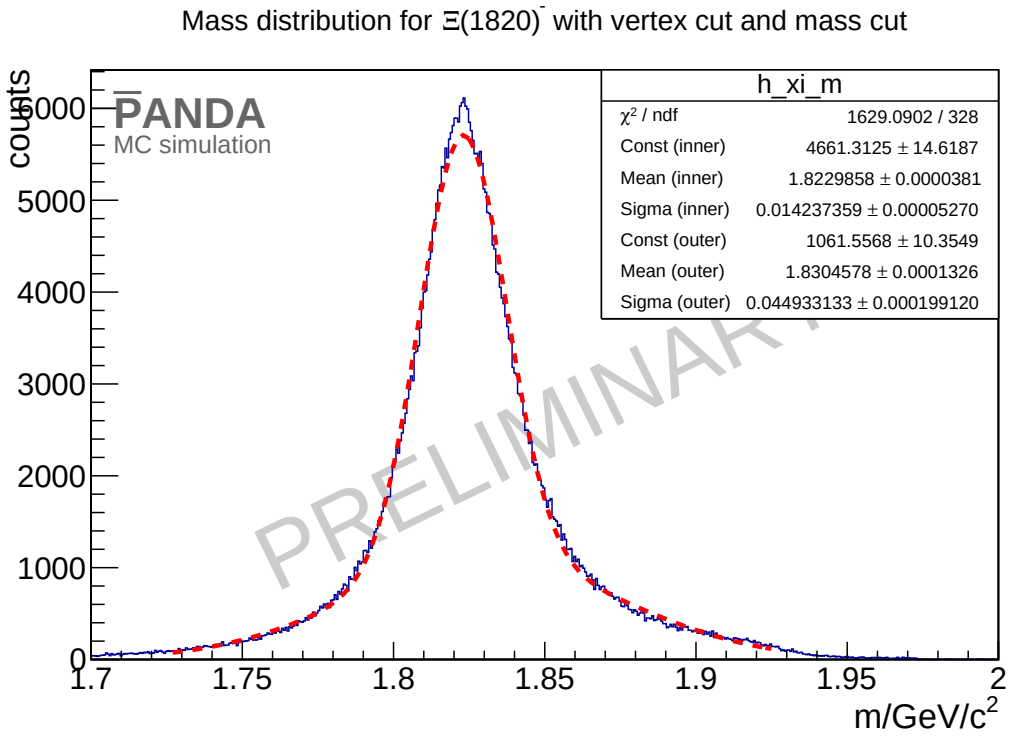

Figure 2.22: "PROPOSED FOR RELEASE" Mass distribution (blue line) after all cuts for Ξ(1820). The performed double Gaussian fit is shown as red dashed line.

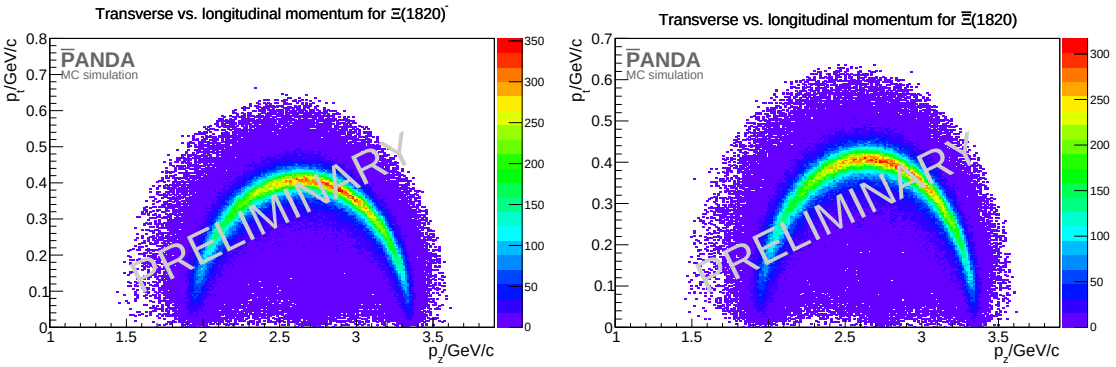

(a) Ξ(1820) (b) Ξ̄(1820)

Figure 2.23: "PROPOSED FOR RELEASE" Both plots show the longitudinal versus the transverse momentum of the excited cascade baryon.

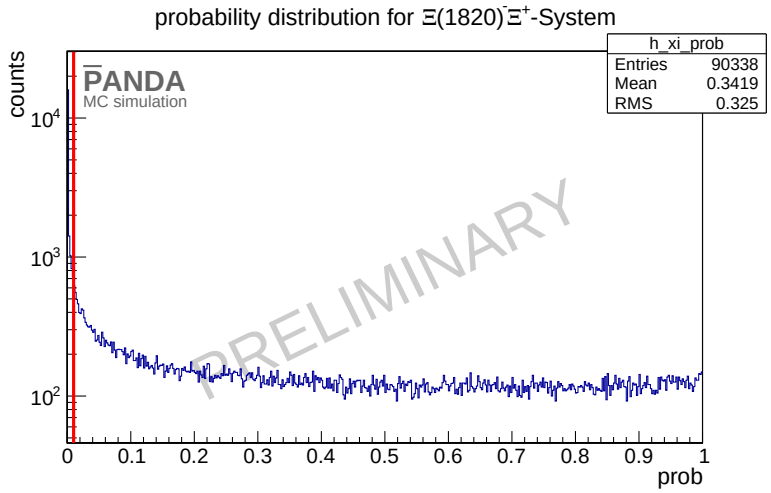

Figure 2.24: "PROPOSED FOR RELEASE" 4-constraint fit probability. The red line denotes the cut value of 1%.

Table 2.5: "PROPOSED FOR RELEASE" reconstruction efficiency for non-final state particles for $\bar{p}p \to \Xi(1820)\,\bar{\Xi}$

particle	reco. efficiency in %	dp/p in %
Λ^0	50.3278	1.50497
$\bar{\Lambda}^0$	41.4625	1.45024
$\bar{\Xi}$	18.389	1.2889
$\Xi(1820)$	32.0245	2.67691
$\Xi(1820)\,\bar{\Xi}$ system	4.69293	1.03214

$$(p_x,\, p_y,\, p_z,\, E) = (0,\, 0,\, 4.6,\, 5.63)$$

of the $\bar{p}p$. This fit is performed with the PndKinFitter. After the four-momentum fit only those candidates are selected which have a χ^2 probability of more than 1%. The χ^2 probability is shown in figure 2.24. The red line denotes the cut value.

The selection scheme is shown in figure 2.25

Results

The results of the reconstruction efficiency for all non-final state particles is shown in table 2.5 and table 2.6.

Figure 2.26 shows the Dalitz plot for the $\bar{\Xi}$, Λ^0 and K^- final states after the reconstruction. Compared with the Dalitz plot of the simulated particles shown in figure 1.4 the

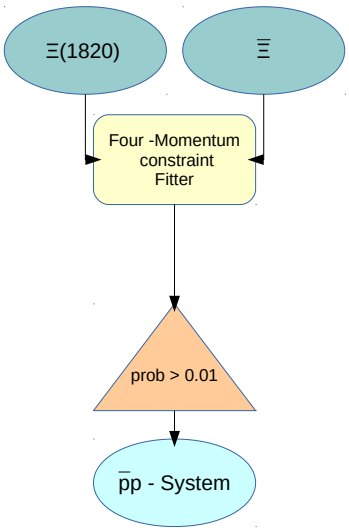

Figure 2.25: "PROPOSED FOR RELEASE" Scheme for the reconstruction of the hole reaction chain.

Table 2.6: "PROPOSED FOR RELEASE" reconstruction efficiency for non-final state particles for $\bar{p}p \rightarrow \bar{\Xi}(1820)\,\Xi$

particle	reco. efficiency in %	dp/p in %
Λ^0	42.4693	1.45429
$\bar{\Lambda}^0$	48.9991	1.50196
Ξ	18.6405	2.29877
$\bar{\Xi}(1820)$	33.2238	1.31081
$\bar{\Xi}(1820)\,\Xi$ system	4.87227	1.03127

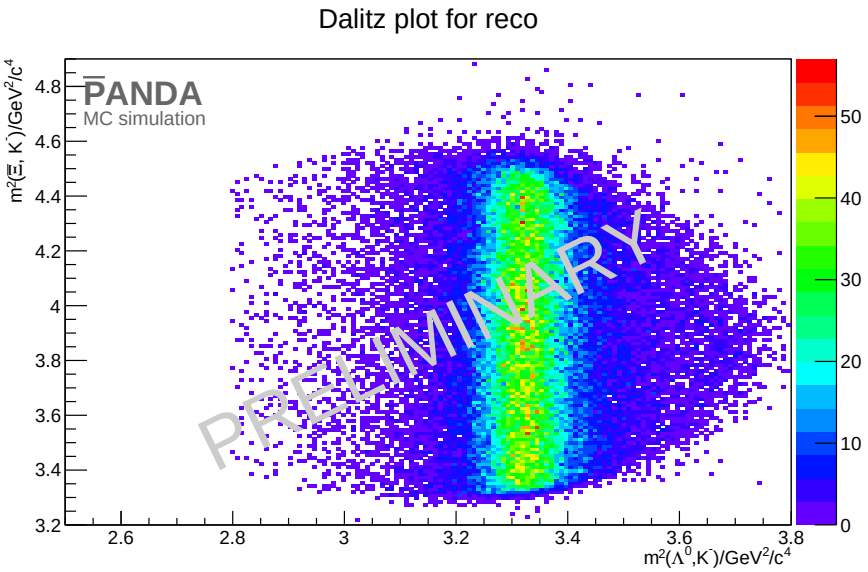

Figure 2.26: "PROPOSED FOR RELEASE" Dalitz plot for reconstructed particles

143 reconstruction seems to be good.

3 Background

For background studies 15 million events are simulated with the Dual Parton Model based generator DPM. To make the selected events of background and signal comparable a scaling factor is needed. This scaling factor can be calculated with the number of generated events and the cross section of signal and background.

$$B = \frac{N_{\mathrm{sig}} / \left(\sigma_{\mathrm{sig}} \cdot \mathrm{Br}\right)}{N_{\mathrm{bg}} / \sigma_{\mathrm{bg}}}, \tag{3.0.1}$$

where N_{sig} is the number of generated signal events, N_{bg} the number of generated background events and Br the branching ratio. The cross section are given by $\sigma_{\mathrm{sig}} = 1\,\mu\mathrm{b}$ and $\sigma_{\mathrm{bg}} = 50\,\mathrm{mb}$ [1]. The scaling factor is different for each particle. In table 3.1 the scaling factors are shown for the channel $\bar{\mathrm{p}}\mathrm{p} \to \Xi\,(1820)\,\bar{\Xi}$. The scaling factors for the c.c. channel are the same.

All background events are reconstructed like the signal events. The number of reconstructed Background events is shown in table 3.2.

Multiplying the number of background events with the corresponding scaling factor make them comparable with the number of signal events. The comparison between signal and background events is shown in table 3.3. The significance is given by

$$S = \frac{N_{\mathrm{sig}}^2}{N_{\mathrm{sig}} + N_{\mathrm{bg}}},$$

where N_{bg} is scaled with B.

The number of simulated background events is too small to make a useful comparison between the number of signal and background events. Further background studies for this

Table 3.1: Scaling factor B of each particle type for the channel $\bar{\mathrm{p}}\mathrm{p} \to \Xi\,(1820)\,\bar{\Xi}$.

Particle	Scaling factor
Λ^0	7,828.16
$\bar{\Xi}$	7,837.01
$\Xi\,(1820)$	7,837.01
$\Xi\,(1820)\,\bar{\Xi}$	12,269.89

Table 3.2: Number of reconstructed background events for $\bar{p}p \to \Xi(1820)\,\bar{\Xi}$

Particle	N_{bg}
Λ^0	264,142
$\bar{\Lambda}^0$	124,068
$\bar{\Xi}$	3,062
$\Xi(1820)$	298
$\Xi(1820)\,\bar{\Xi}$	0

Table 3.3: "PROPOSED FOR RELEASE" The number of background events compared to the number of signal events for $\bar{p}p \to \Xi(1820)\,\bar{\Xi}$.

Particle	N_{sig}	$N_{bg} \cdot B$	S
Λ^0	786,243	$264,142 \cdot B_{\Lambda^0}$	298.85
$\bar{\Lambda}^0$	711,820	$124,068 \cdot B_{\bar{\Lambda}^0}$	521.32
$\bar{\Xi}$	302,681	$3,062 \cdot B_{\bar{\Xi}}$	3770.26
$\Xi(1820)$	490,672	$298 \cdot B_{\Xi(1820)}$	85,191.23
$\Xi(1820)\,\bar{\Xi}$	74523	0	

reaction chain and its charged conjugated channel have to be done as a next step.

4 Summary and Conclusion

The reconstruction of signal events is very well. The hole reaction chain can be reconstructed with an efficiency of nearly 5% for both channels.
Final states particles have a reconstruction efficiency of nearly 80%. The reconstruction of Λ^0 and $\bar{\Lambda}^0$ shows a difference in the efficiencies. This is caused by the different mother particles of the Λ^0 and $\bar{\Lambda}^0$. The reconstruction efficiency for Λ^0 and $\bar{\Lambda}^0$ could be improved by using lambda discs. But this has to be check and is one of the next steps in this analysis.
The reconstructed mass for $\Xi\,(1820)$ and $\bar{\Xi}\,(1820)$ is in a good agreement with the literature value coming from [2].
The topology of the decay chain suppresses the background efficiently without optimizing any cut. The comparison between the number of signal and background events shows how good background events could be suppressed by the selection. To be able to make a useful comparison between these numbers, more background events have to be simulated.

References

[1] W. Erni, I. Keshelashvili, B. Krusche, M. Steinacher, Y. Heng, Z. Liu, H. Liu, X. Shen, O. Wang, H. Xu, *et al.*, "Physics performance report for panda: Strong interaction studies with antiprotons," *arXiv preprint arXiv:0903.3905*, 2009.

[2] J. B. et al., *Particle Data Group.* Phys. Rev. D86, 010001, 2012.